INTERNATIONAL JOURNAL FOR NUMERICAL METHODS IN FLUIDS
Int. J. Numer. Meth. Fluids 2003; **42**:249–263 (DOI: 10.1002/fld.485)

Chebyshev super spectral viscosity solution of a two-dimensional fluidized-bed model

Scott A. Sarra*,†

Department of Mathematics, Marshall University, One John Marshall Drive, Huntington, WV 25755-2560, U.S.A.

SUMMARY

The numerical solution of a model describing a two-dimensional fluidized bed by a Chebyshev super spectral viscosity (SSV) method is considered. The model is in the form of a hyperbolic system of conservation laws with a source term, coupled with an elliptic equation for determining a stream function. The coupled elliptic equation is solved by a finite-difference method. The mixed SSV/finite-difference method produces physically shaped bubbles, on a very coarse grid. Fine scale details, which were not present in previous finite-difference solutions, are present in the solution. Copyright © 2003 John Wiley & Sons, Ltd.

KEY WORDS: fluidized bed; multiphase flow; pseudospectral; spectral viscosity

1. INTRODUCTION

Fluidized beds are used in the chemical and fossil fuel processing industries to mix particulate solids and fluids (gases or liquids). A typical fluidized bed consists of a vertically oriented chamber, a bed of particulate solids, and a fluid flow distributor at the bottom of the chamber. The fluid flows upward through the particles creating a force that counteracts gravity at which time a state of minimum fluidization is reached. Stronger gas inflows (more than is necessary to maintain minimum fluidization) lead to pockets of gas, or equivalently low particle concentrations, resembling bubbles in a liquid travelling upward through the particles. Each rising bubble pushes a large amount of mass in front of it. Particles move downward through and around the rising bubble until it reaches the top of the bed. A settled bed is reestablished, and the cycle repeats. Each set of upward moving particles is referred to as a slug.

* Correspondence to: S. A. Sarra, Department of Mathematics, Marshall University, One John Marshall Drive, Huntington, WV 25755-2560, U.S.A.
† E-mail: scott@scottsarra.org

Received 10 May 2002
Revised 16 December 2002

In this paper, a two-dimensional fluidized-bed model in the form of a hyperbolic system of conservation laws with a source term (1), coupled with an elliptic equation (2) for determining a stream function, is solved numerically.

$$w_t + f(w)_x + g(w)_z = b(w, \psi_x, \psi_z) \tag{1}$$

$$-(\psi_{xx} + \psi_{zz}) + p(x,z)\psi_x + q(x,z)\psi_z = r(x,z) \tag{2}$$

The origins of the model can be found in [1] where a general set of equations modelling dispersed two-phase flow is derived. In Reference [2] a stream function is introduced into the model which corresponds to the total volumetric flux. In the paper [3], the authors state the model for the case of heavy particles dispersed in a gas and with the gas inertia being neglected. It is in this form that we consider the model. A distinguishing feature of the model is that it neglects particle viscosity. Mathematical models of fluidized beds may or may not include a particle viscosity term in an attempt to model the property of the fluidized particles that resists the force tending to cause them to flow. It has been speculated by some authors [4] that particle viscosity, no matter how small, is essential for the behaviour corresponding to slugging to occur. However, it has been demonstrated numerically for a one-dimensional model [5–7] and for the considered two-dimensional model [3, 8], that a model without particle viscosity is capable of reproducing oscillatory slugging behaviour.

Much of the early numerical work with fluidized-bed models produced results, particularly bubble shape, which did not agree with experimental observations (see Reference [9] and references within). Often, the models which were used included particle viscosity. Recently, the particle viscosity free model, was solved numerically by a second-order Godunov method which produced a numerical solution which included the physically observed kidney-shaped bubble [3].

Our interest in using the Chebyshev super spectral viscosity method is to see if a realistic bubble shape can be realized while using coarser grids than second-order finite-difference methods required. Also, it is of interest to see if the spectral method can reveal any small scale structures in the flow that the finite-difference methods could not. Since the formation of a bubble in fluidized beds has been shown to correspond mathematically to the formation of a shock [10], the standard Chebyshev collocation method will not converge to the entropy solution [11]. Thus, the addition of spectral viscosity will be necessary. This work focuses on extending the Chebyshev super spectral viscosity (SSV) method that was successfully used on a one-dimensional fluidized-bed model [7] to a two-dimensional fluidized-bed model.

This paper is organized as follows: In Section 2, the Chebyshev collocation method and Chebyshev super spectral viscosity methods are reviewed. Section 3 describes the fluidized-bed model and numerical results are presented in Section 4.

2. CHEBYSHEV SUPER SPECTRAL VISCOSITY METHOD

The standard collocation points for a Chebyshev collocation (Pseudospectral) method are usually defined by

$$x_j = -\cos\left(\frac{\pi j}{N}\right), \quad j = 0, 1, \ldots, N \tag{3}$$

These points are extrema of the Nth-order Chebyshev polynomial,

$$T_k(x) = \cos(k \arccos(x)) \tag{4}$$

The points are often labelled the Chebyshev–Gauss–Lobatto (CGL) points, a name which alludes to the role of the points in certain quadrature formulas. The CGL points cluster quadratically around the endpoints and are less densely distributed in the interior of the domain.

The Chebyshev collocation method is based on assuming that an unknown PDE solution, u, can be represented by a global, interpolating, Chebyshev partial sum,

$$u_N(x) = \sum_{n=0}^{N} a_n T_n(x) \tag{5}$$

The discrete Chebyshev coefficients, a_n, are defined by

$$a_n = \frac{2}{N} \frac{1}{c_n} \sum_{n=0}^{N} \frac{u(x_j) T_n(x_j)}{c_j} \quad \text{where } c_j = \begin{cases} 2 & \text{when } j = 0, N \\ 1 & \text{otherwise} \end{cases} \tag{6}$$

Derivatives of u at the collocation points are approximated by the derivative of the interpolating polynomial evaluated at the collocation points. The first derivative, for example, is defined by

$$\frac{\mathrm{d}u}{\mathrm{d}x} = \sum_{n=0}^{N} a_n^{(1)} T_n(x) \tag{7}$$

Since $a_{N+1}^{(1)} = 0$ and $a_N^{(1)} = 0$, the non-zero derivative coefficients can be computed in decreasing order by the recurrence relation:

$$c_n a_n^{(1)} = a_{n+2}^{(1)} + 2(n+1) a_{n+1}, \quad n = N-1, \ldots, 1, 0 \tag{8}$$

The transform pair given by Equations (5) or (7) and (6) can be efficiently computed by a fast cosine transform. Equivalently, the interpolating polynomial and its derivatives can be computed in physical space using matrix multiplication [12]. Special properties of the Chebyshev basis allow for differentiation via parity matrix multiplication [13] (even–odd decomposition [14]), which can be performed by using slightly more than half as many floating point operations as standard matrix multiplication. More detailed information may be found in the standard references [11, 15–19].

After the spectral evaluation of spatial derivatives, the system of ordinary differential equations

$$\frac{\mathrm{d}\mathbf{u}}{\mathrm{d}t} = F(\mathbf{u}, t)$$

results, where $\mathbf{u}$ is the vector containing the unknown PDE solution at the collocation points. The system is typically integrated by a second-, third-, or fourth-order explicit Runge–Kutta method to advance the solution in time.

A co-ordinate transformation may be necessary either to map a computational interval to $[a,b]$ from the interval $[-1,1]$, or to redistribute the collocation points within an interval for the purpose of giving high resolution to regions of very rapid change. Perhaps the most popular map used to redistribute the CGL points (3) is the Kosloff/Tal-Ezer map [20]

$$x = g(\xi,\gamma) = \frac{\arcsin(\gamma\xi)}{\arcsin(\gamma)} \tag{9}$$

If the PDE solution contains shocks, the spectral collocation method will not converge to the correct entropy solution [11]. In this case, a spectrally small viscosity term, as defined in Reference [10], must be added in order to stabilize the approximation and ensure convergence to the entropy solution. This can be done without sacrificing spectral accuracy and can be accomplished in several different ways, with each way being labelled a particular type of spectral viscosity method. We have used the SSV method of Reference [21], which for a conservation law in one space dimension, can be stated as

$$\frac{\partial}{\partial t} u_N + \frac{\partial}{\partial x} f(u_N) = \varepsilon(-1)^{s+1} Q^{2s} u_N = \mathrm{SSV}(s,C,N) \tag{10}$$

where the viscosity operator is given by

$$Q = \sqrt{1-x^2}\,\frac{\partial}{\partial x} \tag{11}$$

and $\varepsilon = CN^{1-2s}$. The notation $\mathrm{SSV}(s,C,N)$ is used to indicate that the strength of viscosity term depends on the parameters s, C and N. It was shown in Reference [21] that if the parameter C is chosen large enough to ensure stability and such that $0 \leqslant C \leqslant N^{1/2}$, and if s is chosen such that $s \leqslant \ln(N)$, that the bounded solutions of (10) will converge to the correct entropy solution. Except for the ranges mentioned in order to ensure convergence to the entropy solution, the parameters s and C are problem dependent, depending mainly on the strength of the shocks involved.

A direct implementation of (10) amounts to adding $2s$ spatial derivatives to the equation. This would introduce additional stiffness which would severely limit the stable time step and increase the computational work involved by requiring the computation of higher-order derivatives. Hence, the practical implementation of the SSV method is an important issue. In order to derive an efficient implementation of the SSV method, it is necessary to first examine the viscosity operator Q^2 applied to the Chebyshev polynomial (4), $T_k(x)$.

$$Q^2 T_k(x) = \sqrt{1-x^2}\,\frac{\partial}{\partial x}\left[\sqrt{1-x^2}\,\frac{\partial}{\partial x} T_k(x)\right] = -k^2 T_k(x) \tag{12}$$

As a result of applying the viscosity operator to the Chebyshev polynomials, it can be noticed that the Chebyshev polynomials are the eigenfunctions of the operator Q^2 with eigenvalues k^2. Expanding the viscosity term, which is the right side of (10), we notice that

$$\varepsilon(-1)^{s+1} Q^{2s} u_N = -CN \sum_{k=0}^{N} \left(\frac{k}{N}\right)^{2s} a_k(t) T_k(x) \tag{13}$$

The SSV method can be solved by time splitting. We describe the implementation for a simple splitting which is first-order accurate in time. However, the implementation extends in an obvious way to higher-order split schemes, such as Strang [22] splitting, which we use in the numerical examples. The first-order time splitting based on equations

$$\frac{\partial}{\partial t} u_N + \frac{\partial}{\partial x} f(u_N) = 0 \tag{14}$$

and

$$\frac{\partial}{\partial t} u_N = \varepsilon(-1)^{s+1} Q^{2s} u_N \tag{15}$$

The second equation (15), in the split step can be written as

$$\frac{\partial}{\partial t}\left[\sum_{k=0}^{N} a_k(t) T_k(x)\right] = -CN \sum_{k=0}^{N} \left(\frac{k}{N}\right)^{2s} a_k(t) T_k(x)$$

which can be solved analytically. Over one time step, the analytical solution modifies the Chebyshev coefficients as

$$a_k(t + \Delta t) = a_k(t)\, \exp(-CN\Delta t (k/N)^{2s})$$

Thus, the exact solution of the SSV split step can be written as the filtered partial sum

$$u_N(x) = \sum_{k=0}^{N} \sigma\left(\frac{k}{N}\right) a_k(t) T_k(x) \tag{16}$$

where

$$\sigma\left(\frac{k}{N}\right) = \exp\left(-\alpha \left|\frac{k}{N}\right|^{\beta}\right) \tag{17}$$

is an exponential filter of strength α and order β as described in Reference [23]. The Chebyshev SSV method is equivalent to applying the exponential filter with $\beta = 2s$ and $\alpha = CN\Delta t$. The method and can be implemented with little additional cost. It should be stressed that while the SSV method is being implemented via the exponential filtering framework, that it is not a βth-order filter as it does not meet the requirements set forth in Reference [23]. The amount of damping of the high modes is significantly less with the SSV method than with the application of a βth-order exponential filter. An application of a βth-order exponential filter typically takes $\alpha = -\ln \varepsilon$ where ε is machine zero (on a 32-bit machine using double precision floating point operations, $\varepsilon = 2^{-52}$ and $\ln(\varepsilon) \simeq -36.0437$). Figure 1 compares two exponential filters of different orders with an application of the filter with the parameters set as $\alpha = 0.032$ and $\beta = 4$, which are possible settings that may be used if the filtering framework is used to implement the SSV method.

To extend the Chebyshev SSV method to two dimensions we have used Strang's second-order splitting [22] to reduce the two-dimensional problem (1) to a sequence of one-dimensional problems. We have also used Strang splitting to separate the contribution of the source

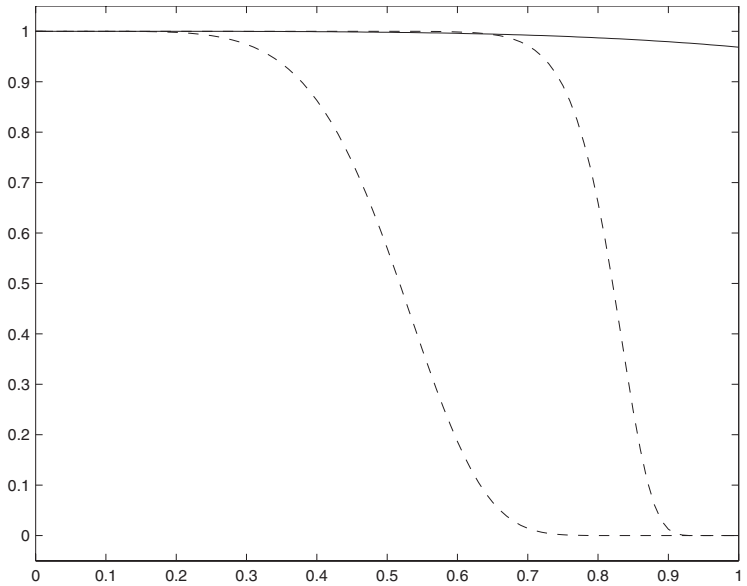

Figure 1. Exp. filter ($\beta = 6$, $\beta = 20$, dashed) vs SSV (solid).

term. The splitting is as follows:

$$w_t = b(w, \psi_x, \psi_z) \tag{18}$$

$$w_t + g(w)_z = 0 \tag{19}$$

$$w_t = \mathrm{SSV}(s, C, N)_z \tag{20}$$

$$w_t + f(w)_x = 0 \tag{21}$$

$$w_t = \mathrm{SSV}(s, C, N)_x \tag{22}$$

$$w_t + g(w)_z = 0 \tag{23}$$

$$w_t = \mathrm{SSV}(s, C, N)_z \tag{24}$$

$$w_t = b(w, \psi_x, \psi_z) \tag{25}$$

Equations (21) and (22) are solved over a full time step while the other 6 equations are evaluated over a time step of size $\Delta t/2$. The fractional steps involving the source terms (18) and (25), may possibly be evaluated in closed form. Otherwise, they may be advanced in time with an ODE integrator. The SSV split steps (20), (22) and (24) can be evaluated exactly as in (16). The remaining equations are advanced in time with a second-order ODE integrator. We have used an explicit second-order Runge–Kutta method in the numerical examples. In

this formulation of the problem, $g(w)_z$ is evaluated 4 times, $f(w)_x$ 2 times, the source term 2 times, SSV_x is applied once, and SSV_z is applied twice, per time step.

From our experience, the spectral viscosity method can also be implemented successfully in an unsplit, fully two-dimensional formulation, without source term splitting. For a suitably chosen time step, the results of the different problem formulations did not noticeably vary in the numerical examples. However, slightly less spectral viscosity was necessary to obtain a stable approximation with the split formulation than with the unsplit formulation. It is speculated that the incremental way in which the spectral viscosity is applied in the split formulation makes this possible.

3. FLUIDIZED BED MODEL

Let $\alpha(x,z,t)$ denote the particle concentration, $m(x,z,t)=\alpha u$ the horizontal momentum, $n(x,z,t)=\alpha v$ the vertical momentum, $u(x,z,t)$ the horizontal velocity, and $v(x,z,t)$ the vertical velocity. The variable x describes the variation along the distributor plate at the bottom of the bed and the variable z describes the vertical direction from the bottom to the top of the bed. The two-dimensional fluidized bed can be described by a system of conservation laws with a source term of form (1) as

$$\alpha_t + m_x + n_z = 0 \tag{26}$$

$$m_t + (mu + F(\alpha))_x + (nu)_z = (1-\alpha)^{-3.5}(\alpha\psi_z - m) \tag{27}$$

$$n_t + (mv)_x + (nv + F(\alpha))_z = -(1-\alpha)^{-3.5}(\alpha\psi_x + n) - \alpha \tag{28}$$

where $F(\alpha)$ is specified as

$$F(\alpha) = s^2\alpha + \frac{s^2\alpha_{\mathrm{p}}^2}{\alpha - \alpha_{\mathrm{p}}} + 2s^2\alpha_{\mathrm{p}}\ln(|\alpha - \alpha_{\mathrm{p}}|) \tag{29}$$

These equations have been non-dimensionalized using v_t, the terminal velocity of an isolated particle as the velocity scale, and v_t^2/g and v_t/g as the length and time scales, respectively, where g is the acceleration due to gravity [3].

The parameter α_0 is the concentration of particles at equilibrium and α_{p} is the packing concentration which sets an upper limit for α where $0<\alpha<1$. The parameter $\alpha_{0\mathrm{u}}$ denotes the particle concentration corresponding the critical state dividing linearly stable and unstable states (the particle concentration at minimum fluidization). The constant $s=3.5(1-\alpha_{0\mathrm{u}})^{2.5}(\alpha_{\mathrm{p}}-\alpha_{0\mathrm{u}})$ is related to the linear stability of the equilibrium solutions which correspond to states of uniform fluidization. The stream function $\psi(x,z,t)$ is defined by the elliptic equation of form (2) with the functions $p(x,z)$, $q(x,z)$ and $r(x,z)$ specified as

$$p(x,z) = -\frac{\alpha_x}{\alpha}\left(1 + \frac{3.5\alpha}{1-\alpha}\right)$$

$$q(x,z) = -\frac{\alpha_z}{\alpha}\left(1 + \frac{3.5\alpha}{1-\alpha}\right)$$

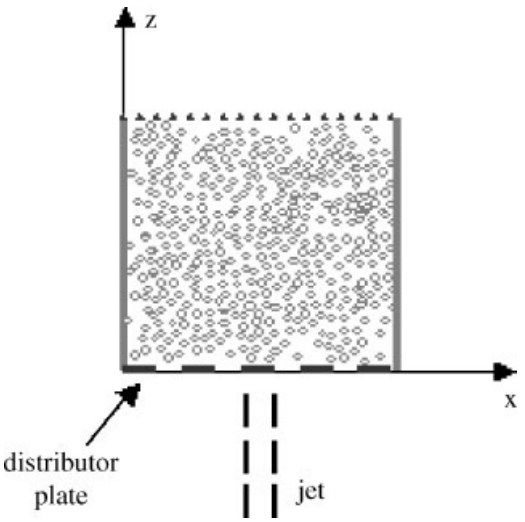

Figure 2. 2d fluidized bed.

$$r(x,z)=\frac{1}{\alpha}\left(n_x-m_z+\frac{3.5}{1-\alpha}[\alpha_x n-\alpha_z m]\right)$$

The scale for the stream function is v_t^3/g.

The computational domain is taken as $(x,z)\in[-x_R,x_R]\times[-z_R,z_R]$. Zero particle momenta in the directions normal to physical boundaries for particles colliding with a wall are applied giving $u=0$ at $x=-x_R$ and x_R and $v=0$ at $z=-z_R$. The boundaries for the elliptic equation at $x=\pm x_R$ are streamlines with constant ψ. At the top of the bed, a somewhat artificial boundary is assumed to exist, where the total volumetric flux is taken to be evenly dispersed. At the bottom of the bed (see Figure 2), a jet of gas of width $2x_b$ is centrally located at the point $(x=0, z=-z_R)$ with the background fluidizing gas entering outside of the jet being $j_M=(1-\alpha_{0u})^{3.5}$. The flux of gas entering through the jet is $j>j_M$ which is specified through the variable α_0 as $j=(1-\alpha_0)^{3.5}$. The described boundary conditions on ψ can be written as $\psi(-x_R,z,t)=0$, $\psi(x_R,z,t)=-2x_R j_M+2x_b(j_M-j)$, $\psi(x,z_R,t)=(-j_M+x_b(j_M-j)/x_R)(x+x_R)$ and

$$\psi(x,-z_R,t)=\begin{cases}-j_M(x+x_R) & -x_R\leqslant x\leqslant -x_b\\ -j(x+xb)-j_M(x_R-xb) & -x_b<x<x_b\\ -j_M(x+x_R)+2x_b(j_M-j) & x_b\leqslant x\leqslant x_R\end{cases}$$

4. NUMERICAL RESULTS

The problem is solved in the split formulation described in Section 2. The fractional steps involving the source term may be evaluated in closed form. By evaluating (18) and (25)

exactly, m and n can be updated as

$$m = \alpha\psi_z(1 - E) + mE \tag{30}$$

and

$$n = \alpha(1 - \alpha)^{3.5}[1 + (1 - \alpha)^{3.5}\psi_x](E - 1) + En \tag{31}$$

where

$$E = \exp\left[\frac{-\Delta t}{2(1 - \alpha)^{3.5}}\right] \tag{32}$$

Since the solution of the equation for the stream may be needed thousands of times during a numerical run, we have not implemented a spectral solution of the elliptic equation. For efficiency we have used a finite-difference method. The solution of the elliptic equation for the stream function is based on fitting a parabola to the data at points, x_{i-1}, x_i and x_{i+1} and then computing the first and second derivatives at x_i. On a uniform grid, the approximation reduces to the standard second-order central differences approximation. The resulting system of algebraic equations is solved by Gauss–Seidel iteration. The streamfunction ψ appears in terms of its first partial derivatives only in Equations (18) and (25). Therefore, Equation (2) is solved initially and then immediately before and after solving Equation (25) at each time step. The derivatives of ψ required in Equations (18) and (25) are found by fitting a parabola to the data at the points x_{i-1}, x_i and x_{i+1}, and then computing the first derivative at x_i. The approximation is second-order accurate on any grid.

A fluidized bed of height and width 3 ($z_R = x_R = 1.5$) units is considered. The initial concentration of particles is taken as $\alpha = \alpha_{0u} = 0.57$ and the initial velocities are $u = v = 0$. At time $t > 0$, a centered jet of gas with a total width of 0.2 units ($x_b = 0.1$), enters from the bottom of the bed.

4.1. Choice of collocation grid

In the first numerical experiment, the gas inflow is specified by setting $\alpha_0 = 0.35$. A 64 by 64 grid is used and the distribution of collocation points is specified three different ways. Three different solutions are obtained, each with a different computational grid. The contours ($\alpha = 0$–0.6) and centre line ($x = 0$) plots are compared at time $t = 3.0$. The goal is to determine which grid best resolves the solution.

The first run uses the CGL grid (3) which clusters points densely around the boundaries and provides poor interior resolution. In order to obtain stable results with the explicit time stepping, it was necessary to take $\Delta t = 0.000025$ and take the SSV parameters as $C = 6$ and $s = 2$. The small time step is typical due to the $O(N^{-2})$ stable time step restriction imposed by the CGL grid. The lack of resolution towards the interior of the domain is apparent from the wide spread contour lines and the centre line plot (Figure 3, top row).

To relax the $O(N^{-2})$ time stepping restriction, a mapped grid specified by map (9) can be used. By taking the map parameter to be $\gamma = 0.86$ in both the x and z directions we end up with a grid with less clustering around the boundaries and with better interior resolution. This setting of the map parameter is theoretically the upper limit of the parameter range that can be used with $N = 64$ in order to maintain a spectral convergence rate [20]. Taking $\Delta t = 0.0001$,

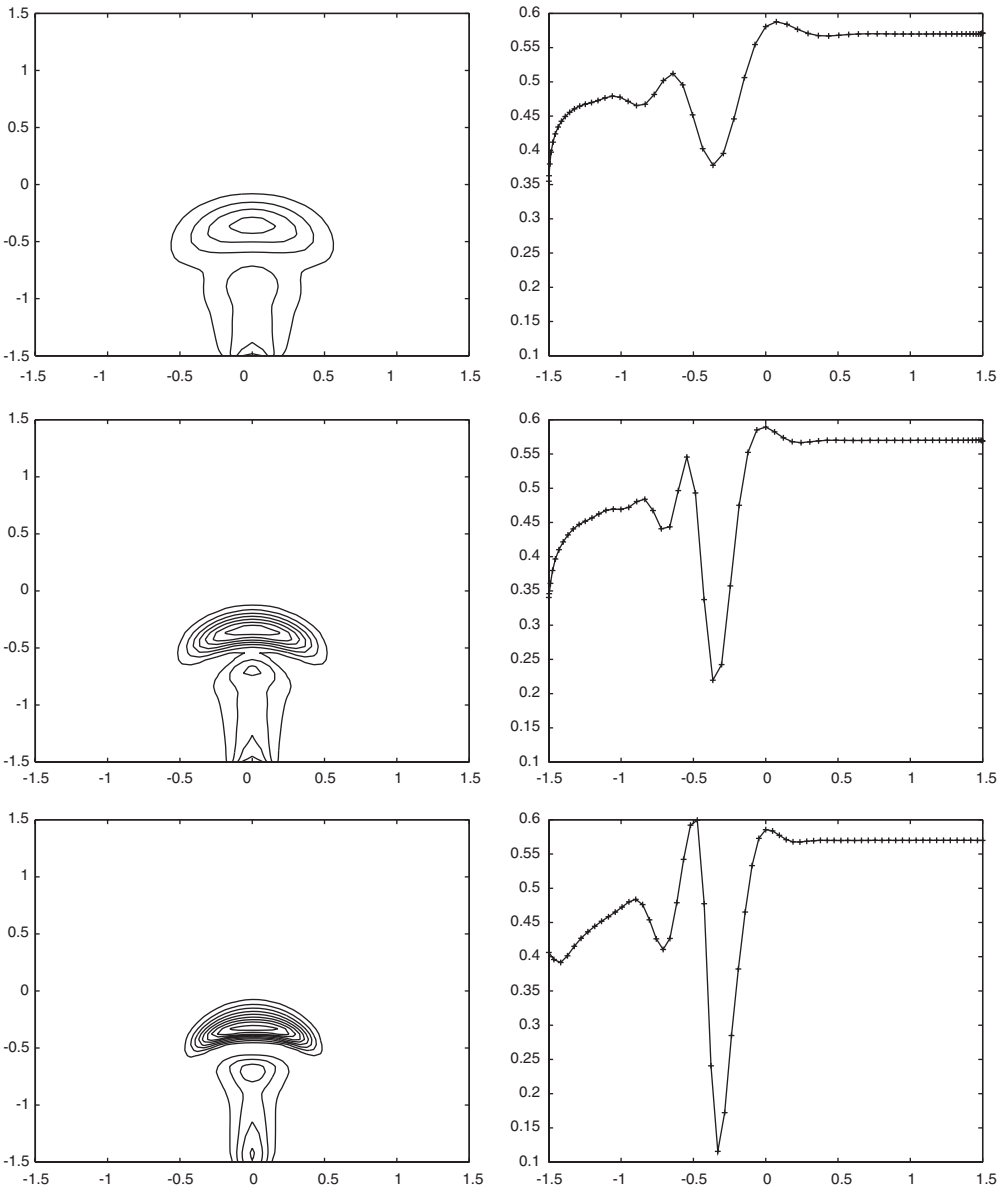

Figure 3. $t = 3.0$, top: CGL grid, middle: $\gamma = 0.86$, bottom: $\gamma = 0.9999$.

and $C = 3$ and $s = 2$, as the SSV parameters, produces stable results. A marked improvement in results can be observed (Figure 3, middle row) when compared with the CGL grid results. Increasing the mapping parameter closer to one produces even better results.

The third run again uses map (9) to specify the grid. The map parameter was chosen as $\gamma = 0.9999$ in both the x and z directions. Choosing the map parameter so close to one results

in a near uniform grid. Taking $\Delta t = 0.0005$, and $C = 3$ and $s = 2$ as the SSV parameters produces stable results. Even though taking γ so large could introduce a mapping error and theoretically sacrifice the spectral convergence rate of the method, this is not an issue in this case as we are implementing a mixed spectral/finite-difference method in which the overall accuracy of the solution will not be spectral. The increased resolution in the interior provided by the near uniform grid is evident (Figure 3, bottom row) in the tightly grouped contour lines. It is concluded that this is the grid that best resolves the problem. The grid allows for the largest stable explicit time step and values of the SSV parameters which result in the smallest amount of spectral viscosity being applied. Compared with the CGL grid results from the first run, the third run used a time step 20 times larger and a spectral viscosity that was only half as strong.

4.2. Grid size

Map (9) is used to form the grid with $\alpha_m = 0.9999$ in both the x and z directions. The map produces a near uniform grid and allows for good resolution in the centre of the domain as well as permitting a relatively large stable time step to be taken. The parameter α_0 is set to $\alpha_0 = 0.2$ which corresponds to a strong gas inflow. The flow is stronger than that which is required to maintain a state of minimum fluidization and slugging in the bed is expected. In the left column of Figure 4, contour plots show α ranging from 0.05 to 0.4 in 0.05 unit increments from time $t = 2.0$ to 4.0 in one unit increments. The set-up for this problem is similar to experiments run in Reference [3] where the numerical solution was by Roe's method which required a 100 by 100 grid to resolve the flow. The spectral method resolves the flow well on this very coarse grid and a physically correct bubble shape is obtained. The simulation exhibits features observed in fluidized beds, such as coalescence, when a smaller bubble catches up to and is absorbed by the main bubble. The SSV parameters in both the x and z directions were $s = 2$ and $C = 1$, which applies only a very weak high pass filter to the spectral solution.

The fact that the flow is well resolved on the 32 by 32 grid indicates that the second-order finite-difference approximation of the stream function is adequate. It seems as if the accuracy in which the flux derivatives are evaluated in the system of conservation laws is the most important factor in obtaining a resolved solution. The 32 by 32 spectral solution produced solutions of similar quality as the finite-difference solutions in Reference [3], but at a fraction of the computational effort, and used significantly less storage space. In Figure 5, counter-rotating convective rolls behind the main bubble are very evident in the velocity field of the coarse grid SSV solution.

The same experiment that was run on the 32 by 32 grid is repeated on a 64 by 64 grid. The results (the right column of Figure 4) on the finer grid are similar to the results obtained on the coarse grid, but some small-scale details in the flow were revealed that were not present in the coarse grid spectral solution or in the finite-difference solutions in Reference [3]. The SSV parameters in both the x and z directions were $s = 2$ and $C = 3$. In the simulation, a small disturbance below the main bubble appears and eventually coalesces with the main bubble. At time $t = 3.0$ (Figure 4, centre right), the formation of two small satellite bubbles is noticeable. By time $t = 4.0$ (Figure 4, bottom right) the main bubble has shed the two satellite bubbles. Figure 6 shows the $t = 4.0$, $\alpha = 0.4$ contour from Figure 4 with the streamlines corresponding to the total volumetric flux superimposed.

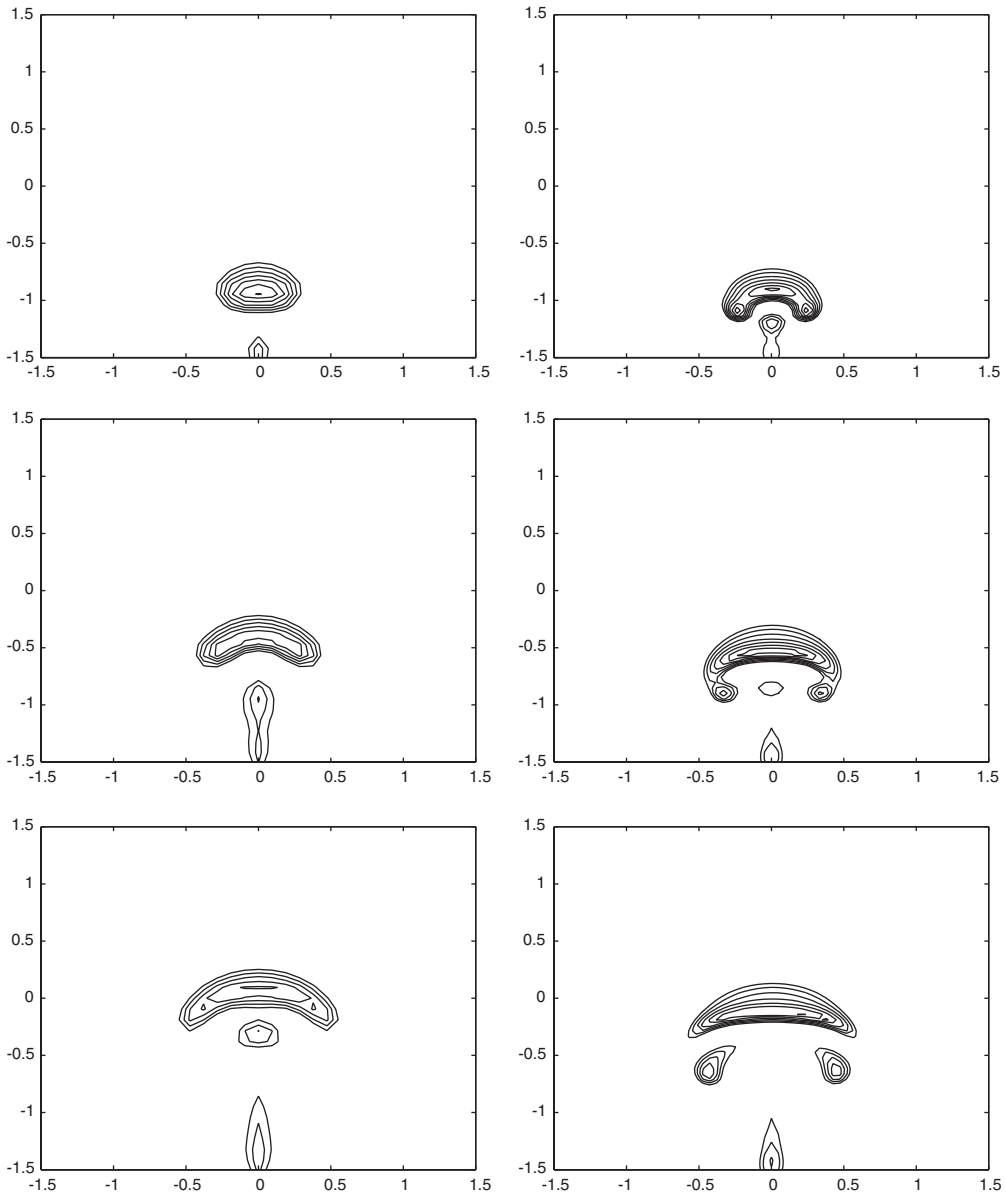

Figure 4. 32 by 32 (left), 64 by 64 (right); $t = 2.0$ (top), $t = 3.0$, $t = 4.0$.

The next result shows that we are approaching a grid-independent solution on a 64 by 64 grid. When going from a resolution of 32 by 32 to a resolution of 64 by 64 there is a difference in both the shape and location of the bubble. Runs with grid densities greater than 64 by 64 produced bubbles with nearly the identical shape and location as the 64 by 64 runs. Additionally, no new fine scale details, such as satellite bubbles appeared at finer

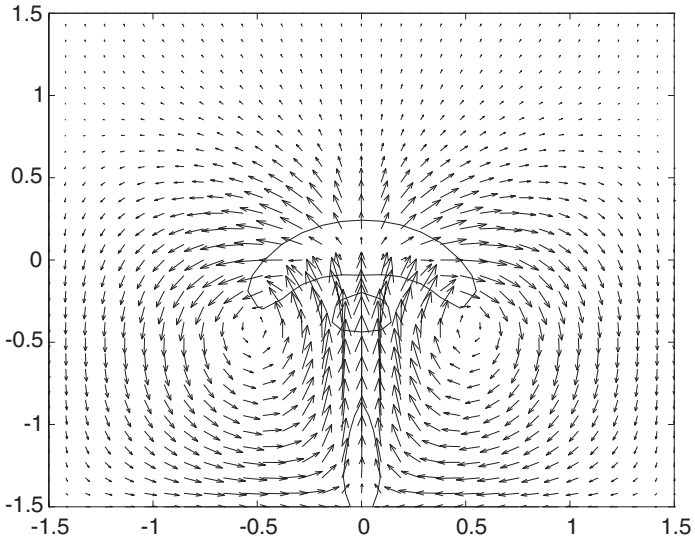

Figure 5. 32 by 32 grid velocity field, $t = 4.0$.

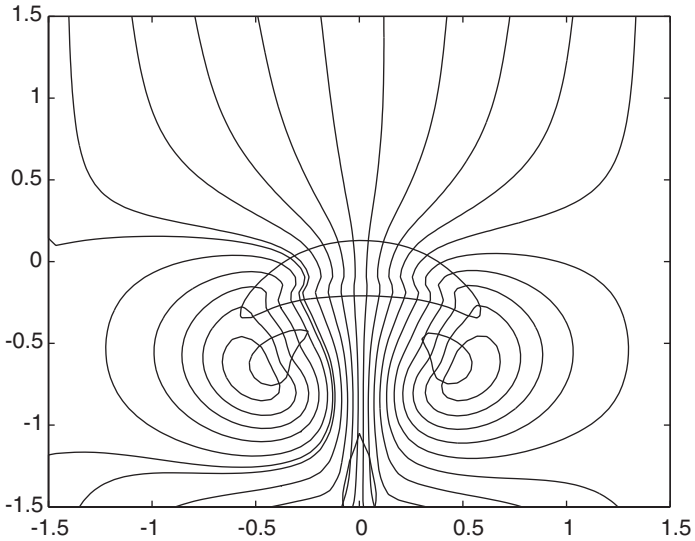

Figure 6. $\alpha = 0.4$ bubble contour with streamlines.

resolutions. Figure 7 compares the centre line ($x = 0$) plots of the 32 by 32 (dotted) and 64 by 64 (dashed) concentration solutions from Figure 4 at time $t = 3.0$. The solid line in Figure 7 is from a 96 by 96 grid calculation which used a grid mapping parameter of $\alpha_m = 0.9999$ and SSV parameters of $s = 2$ and $C = 5$. Except for the chaotic region near the jet at the bottom of the bed, the 64 by 64 and 96 by 96 runs agree very well.

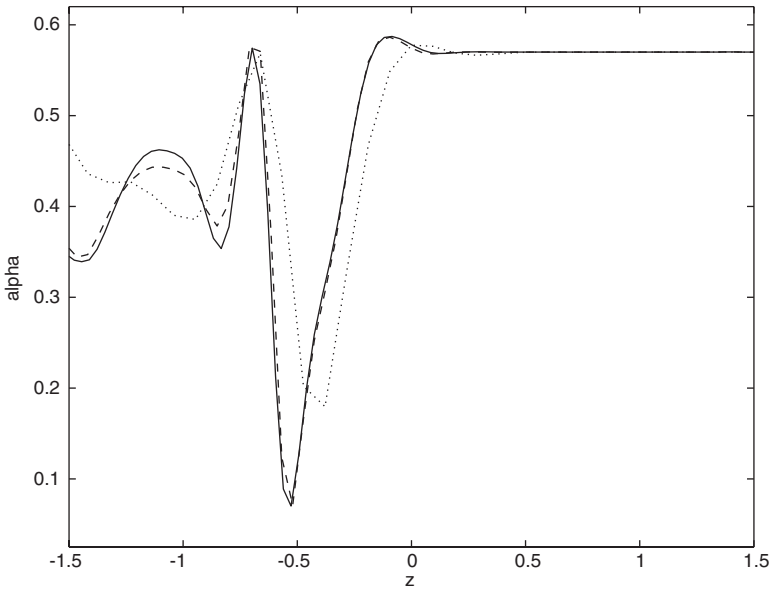

Figure 7. $t = 3.0$, $N = 96$ solid, $N = 64$ dashed, $N = 32$ dotted.

5. CONCLUSIONS

A mixed Chebyshev SSV/finite-difference method has been implemented for the fluidized-bed model. The flux derivatives in the conservation laws are evaluated by a Chebyshev pseudospectral method while the elliptic equation for the stream function is solved by a second-order finite-difference method. The approximation is second-order accurate in time. The SSV method has been shown to produce quality numerical solutions of a complicated multiphase flow problem. The method was able to use fewer degrees of freedom and still resolve fine scale features in the solution better than in previous reported results in Reference [3] using Roe's method with a Superbee flux limiter. A grid which was nearly uniform best resolved the problem, allowed the smallest amount of spectral viscosity to be applied, and allowed the largest stable time step to be used.

Although the development of bubbles in fluidized beds has been shown to mathematically correspond to the development of shocks, spurious oscillations are not visibly evident in the numerical solution. This is in contrast to the Chebyshev SSV solution of a one-dimensional fluidized-bed model in Reference [7] where a post-processing method was used to remove the effects of the Gibbs phenomenon from the approximation. The shocks seem much weaker in the two-dimensional model and the mild filtering of the SSV methods seems to keep any spurious oscillations under control. If an oscillatory solution was obtained, methods for post-processing two-dimensional functions [24, 25] are available. However, theoretically, the results of their application to the two-dimensional fluidized-bed solution would be less certain due to the second-order finite-difference solution of the equation for the stream.

Our future work will consider axisymmetric geometry, and multiple, interacting bubbles. Additionally, higher-order methods for the solution of the stream equation will be explored with the goal of obtaining a solution that has overall spectral accuracy in space.

REFERENCES

1. Drew DA. Mathematical modelling of two-phase flow. *Annual Review of Fluid Mechanics* 1983; **15**:261–291.
2. Ganser G, Li D. Solutions for a two-dimensional hyperbolic-elliptic coupled system. *SIAM Journal of Mathematical Analysis* 1996; **27**(4):1024–1037.
3. Christie I, Ganser GH, Wilder JW. Numerical solution of a two-dimensional fluidized bed model. *International Journal for Numerical Methods in Fluids* 1998; **28**:381–394.
4. Needham D, Merkin J. The propagation of a voidage disturbance in a uniformly fluidized bed. *Journal of Fluid Mechanics* 1983; **131**:427–454.
5. Christie I, Ganser GH, Sanz-Serna JM. Numerical solution of a hyperbolic system of conservation laws with source term arising in a fluidized bed model. *Journal of Computational Physics* 1991; **93**(2):297–311.
6. Christie I, Palencia C. An exact Riemann solver for a fluidized bed model. *IMA Journal of Numerical Analysis* 1991; **11**:493–508.
7. Sarra SA. Chebyshev super spectral viscosity method for a one-dimensional fluidized bed model. *Journal of Computational Physics* 2003; to appear.
8. Sarra SA. Chebyshev pseudospectral methods for conservation laws with source terms with applications to multiphase flow. *Ph.D. Thesis*, West Virginia University, 2002.
9. Syamlal M. High order discretization methods for the numerical simulation of fluidized beds. *AICHE Symposium Series*, vol. 94(318). 1998.
10. Gidaspow D. *Multiphase Flow and Fluidization*. Academic Press: New York, 1994.
11. Tadmor E. Convergence of spectral methods for nonlinear conservation laws. *SIAM Journal of Numerical Analysis* 1989; **26**:30–44.
12. Canuto C, Hussaini MY, Quarteroni A, Zang TA. *Spectral Methods for Fluid Dynamics*. Springer: New York, 1988.
13. Boyd JP. *Chebyshev and Fourier Spectral Methods* (2nd edn). Dover Publications, Inc.: New York, 2000.
14. Solomonoff A. A fast algorithm for spectral differentiation. *Journal of Computational Physics* 1992; **98**: 174–177.
15. Fornberg B. *A Practical Guide to Pseudospectral Methods*. Cambridge University Press: New York, 1996.
16. Funaro D. *Polynomial Approximation of Differential Equations*. Springer: New York, 1992.
17. Gottlieb D, Orszag SA. *Numerical Analysis of Spectral Methods*. SIAM: Philadelphia, PA, 1977.
18. Gottlieb D, Hussaini MY, Orszag SA. Theory and application of spectral methods. In Voigt RG, Gottlieb D, Hussaini MY (eds). *Spectral Methods for Partial Differential Equations*. SIAM: Philadelphia, PA, 1984; 1–54.
19. Trefethen LN. *Spectral Methods in Matlab*. SIAM: Philadelphia, PA, 2000.
20. Kosloff R, Tal-Ezer H. A modified Chebyshev pseudospectral method with an $O(1/N)$ time step restriction. *Journal of Computational Physics* 1993; **104**:457–469.
21. Ma H. Chebyshev-Legendre super spectral viscosity method for nonlinear conservation laws. *SIAM Journal of Numerical Analysis* 1998; **35**:893–908.
22. Strang G. On the construction and comparison of difference schemes. *SIAM Journal of Numerical Analysis* 1968; **5**(3):506–517.
23. Vandeven H. Family of spectral filters for discontinuous problems. *SIAM Journal of Scientific Computing* 1991; **6**:159–192.
24. Gelb A. A hybrid approach to spectral reconstruction of piecewise smooth functions. *Journal of Scientific Computing* 2001; **15**:293–322.
25. Gelb A, Gleeson J. Enhanced spectral viscosity method for the shallow water equations. *Preprint*, 2000.

